IEEE Access
Multidisciplinary | Rapid Review | Open Access Journal

Received 14 August 2023, accepted 23 August 2023, date of publication 31 August 2023, date of current version 7 September 2023.

Digital Object Identifier 10.1109/ACCESS.2023.3310871

RESEARCH ARTICLE

Stochastic Dosimetry Assessment of Human RF-EMF Spatial Exposure Variability in 5G-V2X Vehicular Communication Scenario

MARTA BONATO[1], GABRIELLA TOGNOLA[1], MARTINA BENINI[1,2], (Graduate Student Member, IEEE), SILVIA GALLUCCI[1,2], EMMA CHIARAMELLO[1], SERENA FIOCCHI[1], AND MARTA PARAZZINI[1], (Member, IEEE)

[1]Institute of Electronics, Computer and Telecommunication Engineering (IEIIT), Consiglio Nazionale delle Ricerche (CNR), 20133 Milan, Italy
[2]Department of Electronics, Information and Bioengineering (DEIB), Politecnico di Milano, 20133 Milan, Italy

Corresponding author: Marta Bonato (marta.bonato@ieiit.cnr.it)

This work was financed by Project "EXPOAUTO - Cumulative real smart car exposure to radiofrequency electromagnetic fields in people of different ages from new technologies in automotive services and connected objects" [PNREST Anses, 2020/2 RF/05].

ABSTRACT The present work was focused on assessing the spatial exposure variability for pedestrians on the road, in close proximity to a car equipped with a 5G-V2X antenna, operating at the working frequency of 3.5 GHz and with 3D beamforming capability. Indeed, Cooperative Intelligent Transportation Systems (C-ITS) will soon utilize 5G New-Radio (NR) wireless communication to overcome the limitations of the current V2X (Vehicle-to-Everything) wireless communication technologies, enhancing road-safety and driving efficiency. However, this transition also introduces heterogeneity, uncertainty and variability in the radio frequency (RF) exposure levels of pedestrian and other road-users. To evaluate the spatial exposure variability in these new 5G-V2X scenarios, in this work we adopted an approach which combines a stochastic (metamodeling) technique called Polynomial Chaos Kriging with deterministic dosimetry (classical computation techniques). By utilizing this approach, we were able to assess the exposure levels, expressed in terms of specific absorption rate (*SAR*), for 1000 different beamforming patterns of the 5G-V2X antenna, with low computational cost. The results showed low exposure values compared to ICNIRP guidelines and highlighted a high exposure variability for 5G vehicular communication scenarios.

INDEX TERMS 5G-V2X antenna, cooperative intelligent transport systems, RF human exposure, stochastic dosimetry.

I. INTRODUCTION

In recent years, rapid and widespread technological advancements have been applied in the automotive field to develop a new concept called Cooperative Intelligent Transport Systems (C-ITS) [1]. C-ITS is based on wireless vehicular communications and remote sensing to enhance travel safety, improve transport efficiency, reduce environmental impact and maximize the social and economic benefits of transportation for both the commercial users and the general public [2]. The umbrella of vehicle-to-everything (V2X) wireless communications for C-ITS encompass smart connected vehicles that can communicate with other vehicles (vehicle-to-vehicle, i.e., V2V), pedestrians (vehicle-to-pedestrian, i.e., V2P), infrastructures (vehicle-to-infrastructure, i.e., V2I), and network (vehicle-to-network, i.e., V2N) [3], [4]. The V2X wireless communications operate through two main wireless access technologies: WiFi for mobility, based on the IEEE 802.11p protocol standard in the US or its European equivalent, ITS-G5 [5], and the cellular technology named Cellular-V2X (C-V2X), standardized by the 3rd Generation Partnership Project (3GPP). This includes V2X operated through both the Long-Term Evolution (LTE-V2X) and 5G NR (New Radio) communication

The associate editor coordinating the review of this manuscript and approving it for publication was Jad Nasreddine.

protocol (5G-V2X) [6], [7], [8]. Specifically, the introduction of the 5G NR communication protocol will be proven useful for enabling ultra-reliable low-latency communication close to 99.999%, wider coverage area, improving position accuracy down to 5 cm, as well as high data rate and spectral efficiency for the connected vehicles [2], [9].

To overcome the limitations of LTE-V2X and IEEE 802.11p in terms of low latency, communication speeds and available bandwidth, the 5G NR communication protocol will operate not only in the traditional ITS 5.9 GHz band, but also in two additional, larger frequency ranges: the frequency range 1 (FR1, 410 MHz - 7.125 GHz) and the millimeter waves (mmWaves) frequency range 2 (FR2, 24.25-52.6 GHz) [7], [8]. The successful implementation of 5G-V2X communication will be made possible through the deployment of 5G network infrastructure and the use of innovative technologies, i.e., the use of small-cell networks and massive multiple-input-multiple output (MIMO) base station antenna, the device-to-device (D2D) communication and the application of three-dimensional beamforming (3DBF) techniques [10], [11].

The introduction of new RF frequency ranges and technological changes in 5G wireless network communication is also raising health and safety concerns about human RF exposure levels, as pointed out in the Technical Information Statement (TIS) of the Committee on Man and Radiation (COMAR) [12]. To address these concerns, studies are being conducted on the design and performance characterizations of technological solutions for 5G networks deployment, with a specific focus on its use in the field of C-ITS mobility (see, e.g., [9], [10], [11], [13], [14], [15]). Additionally, studies have also been directed towards the assessment of RF human exposure in these upcoming 5G scenarios. So far, efforts have been made to evaluate RF EMF human exposure to plane wave, dipoles and array antennas in both near-field and far-field conditions using computational methods and considering upcoming 5G mobile network communication scenarios [16], [17], [18], [19]. In the automotive field, a few studies have begun to focus on the assessment of human exposure due to antennas operating at frequencies used in V2X communications [20], [21], [22], [23], and one our previous study specifically assessed the exposure levels of pedestrians in near proximity to a car equipped with two 5G-V2X antennas at 3.5 GHz, where some configurations and orientations between a human model and the car were evaluated thanks to classical computational techniques [24]. However, to the best of our knowledge, none of the previous reported works has taken into account the heterogeneity, uncertainty and variability introduced by the use of these new 5G-V2X communications on RF-EMF human exposure. To address this gap, in the present work we aim to assess the spatial variability of human exposure in a 5G-V2X scenario for the first time. The work was based on a specific case of 5G-V2X scenario, where the innovative technological factors of 5G connectivity were taken into account, i.e., the use of array antenna with varying number of elements, the antenna working frequency at 3.5 GHz, the 3D beamforming capacity and the antenna position on the car body. To obtain the analysis of the spatial variability of human exposure, we use stochastic dosimetry, an approach previously applied in the context of indoor 5G networks, which combines stochastic (metamodeling) techniques with deterministic dosimetry (classical computation techniques), to assess human exposure spatial variability in 5G-V2X scenarios [25].

Briefly, stochastic dosimetry uses statistics to replace expensive computational models with surrogate models, greatly reducing the associated computational costs. Recently, stochastic dosimetry has been applied successfully to assess the variability of EMF exposure assessment in both low and high frequency exposure scenarios (see, e.g., [25], [26], [27], [28], [29], [30], [31], [32]). In stochastic dosimetry, a small number of deterministic simulations obtained from expensive computational dosimetry simulations are coupled with stochastic models to infer the exposure levels in variable scenarios and perform statistics and sensitivity analyses [28].

In the present work, we used a stochastic dosimetry approach called Polynomial Chaos Kriging (PC-Kriging) to take into account the variability of the exposure due to the beamforming capability of a 5G-V2X antenna used in C-ITS mobility, rather than limiting the exposure analysis to a few beamforming patterns of the 5G-V2X antenna. In our previous study [24], we investigated human exposure levels for road users in proximity to a car equipped with 5G-V2X antennas. In [24] we used the deterministic computational dosimetry to assess the exposure; due to the heavy computational load of the method, our previous analysis was limited only to a few specific configurations between the 5G-V2X antenna and the human model. The 5G-V2X antenna was modelled as an array antenna of eight patch elements at the working frequency of 3.5 GHz, in the FR1 (410 MHz - 7.125 GHz) for 5G mobility. By combining deterministic and stochastic approaches, in this work we were able to consider the beamforming capability of the 5G V2X antenna and thus assess human exposure for 1000 different beamforming patterns, with a sustainable computational cost. Exposure was evaluated in terms of the Specific Absorption Rate (*SAR*), that is the RF-EMF power absorbed per unit of mass of the road user, following the International Commission on Non-Ionizing Radiation Protection (ICNIRP) guidelines [33].

II. MATERIALS AND METHODS

We assessed the exposure levels of a human model resembling a pedestrian near a car equipped with a 5G-V2X antenna with 3D beamforming capability. The exposure scenario and the methodology adopted, which required a combination of classical computational method and innovative stochastic dosimetry, are illustrated in Fig. 1 and in Fig. 2, respectively.

In the next sections, we describe in detail the exposure scenario characteristics and the four steps outlined in the workflow of Fig. 2, namely: the ''Exposure Scenario'' section

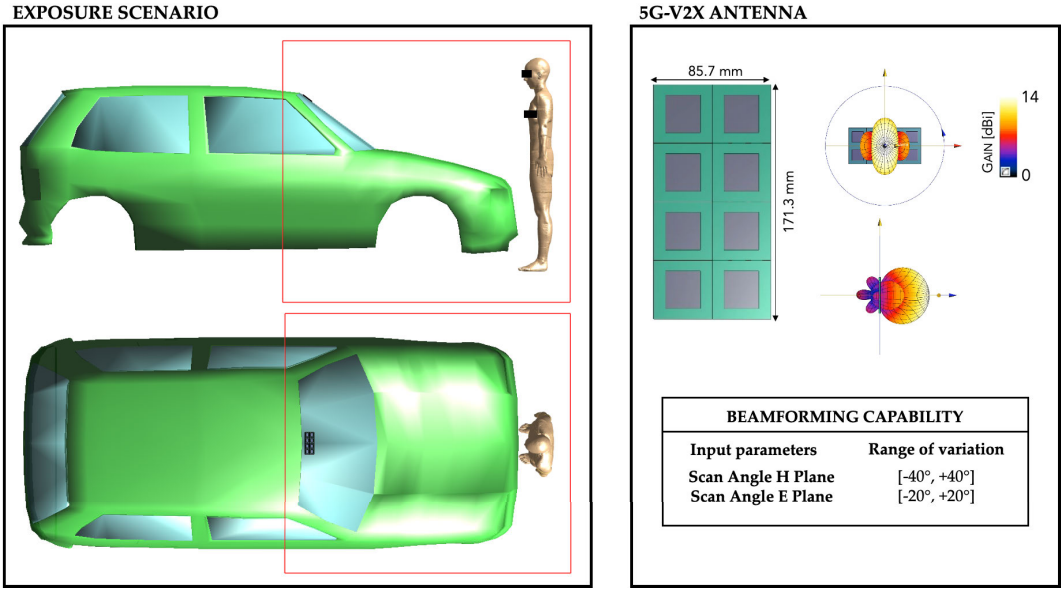

FIGURE 1. On the left, the exposure scenario configuration (the red box indicates the computational domain). On the right, the details of the 5G-V2X antenna and the description of the beamforming capability over the H and E plane and their corresponding ranges.

illustrates the characteristics of the scenario, including the car model, the 5G-V2X antenna model and the human model; the ''Experiment Design'' section motivates the choice for the input settings for the beamforming capability ofV2X antenna and for the deterministic simulations; the ''Stochastic Approach'' section outlines the PC-Kriging approach we used to build the surrogate models; the ''Validation'' section demonstrates the effectiveness of the surrogate models; finally, the ''Exposure Analysis'' section highlights how the surrogate models were applied to assess the *SAR* values in the tissues of interest, with low computational costs.

A. THE EXPOSURE SCENARIO

The exposure scenario analyzed in the current study was the same as in our previous study [24]. The key characteristics of the exposure scenario are summarized here and are illustrated in Figure 1. The car body, which resembles a typical city car model, was modelled using perfect electric conductor (PEC) material and six glass windows (density $\rho = 2500$ kg/m3; conductivity $\sigma = 0.0025$ S/m; relative permittivity $\varepsilon_r = 2.6$). The 5G-V2X antenna, operating at 3.5 GHz for vehicular communication, was modelled as a linear array antenna of eight elements arranged in two rows of four elements each. The design of the antenna was consistent with the technical specifications of the 3GPP Release 16 and Release 17 and the H2020 5G PPP 5G Communication Automotive Research and innovation (5GCAR) Project [7], [8], [34]. Each element of the linear array was modelled as a simple patch antenna with three layers: the ground and patch layers were made of PEC material, whereas the substrate layer was made of dielectric material ($\varepsilon_r = 2.2$ and $\sigma = 0.0005\ S/m$). The patch antenna dimensions equal to $42.8 \times 42.8 \times 4$ mm allowed to achieve the resonance at 3.5 GHz. The 5G-V2X antenna was mounted on the windshield glass, along the midline of the car, in a typical position used in 5G vehicular communication [35], [36]. Differently from our previous study [24], in the current study we examined the impact of the 3D beamforming capability of the 5G-V2X linear array antenna on the exposure levels. Specifically, we set two different scan angles that regulated the beamforming direction in the H-plane (azimuth plane) and in the E-plane (elevation plane). Consistently with the 3D beamforming capability of upcoming 5G network communications antennas [7], [8], [37], we set the beamforming range in the H-plane between $[-40°, +40°]$, where negative scan angles corresponded to beams directed towards the right side of the human model, while in the E-plane the range varied between $[-20°, +20°]$, where negative scan angles corresponded to beams directed towards the ground.

The antenna was driven by a continuous harmonic signal at 3.5 GHz with an input power 1 W and had a radiated efficiency of 98.88%, resulting in a total radiated power equal to 0.9888 W. The anatomical model 'Ella' of the Virtual Family [38] was used, which comprises 76 different tissues and resembles an average adult female (age = 26 years old, height =1.63 m, mass = 57.3 kg, BMI = 21.6 kg/m) [38]. The Ella model was placed in the position that according to the evidence we found in our previous work [24] resulted in the highest exposure, i.e., close to the frontal car hood, at its midline. In this way, the distance between the 5G-V2X antenna and Ella resulted to be around 1.7 m.

B. EXPERIMENT DESIGN

The Step 1 of the workflow in Figure 2 (i.e., $Y = M(\boldsymbol{x})$) is aimed at detecting the input parameters ($\boldsymbol{x}$) and their joint probability functions to characterize the computational model

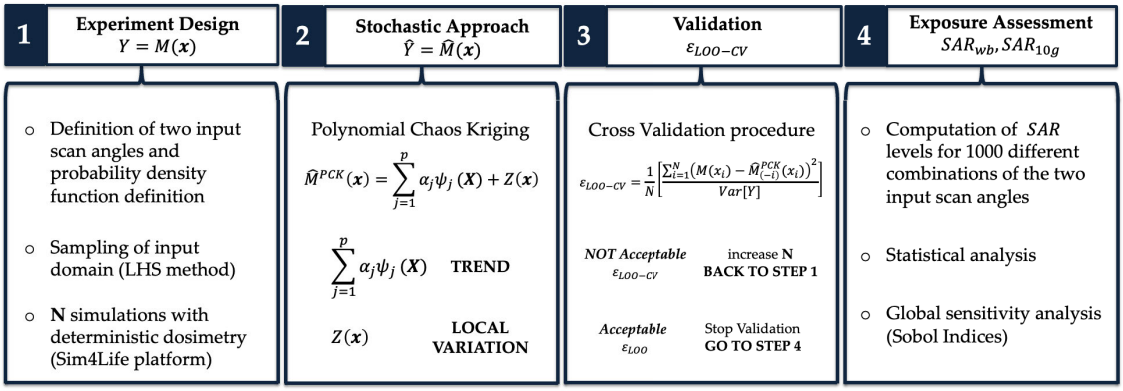

FIGURE 2. Schematic workflow of the methodology used in this paper to assess the RF EMF human exposure spatial variability in 5G-V2X vehicular communication.

M to assess the EMF quantity of interest Y. As previously described, two scan angles were set to characterize the 3D beamforming capability of the 5G-V2X antenna: the scan angle in the H-plane (range variation $[-40°, +40°]$) and the scan angle in the E-plane (range variation $[-20°, +20°]$). The joint probability functions of the two scan angles were hypothesized to be uniformly distributed, since no assumptions were made about the most probable direction of beam of the antenna, to preserve generality. Successively, a Latin hypercube sampling (LHS) method was applied on the joint probability density function of the inputs to generate the input coordinates [28], [31], [39].

These input coordinates were then used as settings for the computational simulations performed using the Sim4Life platform (ZMT Zurich Med Tech AG, Zurich, Switzerland, www.zurichmedtech.com), which implements the finite-difference time-domain (FDTD) solver. The FDTD method represents a direct solution in the time domain of the Maxwell's curl equations, which are discretized by means of a second-order finite-difference approximation both in space and in time in an equidistantly spaced mesh [40]. In the present paper, the computational domain of these simulations (highlighted by the red box in the left part of Fig.1) included half of the car body, the 5G-V2X antenna on the windshield glass, and the entire Ella model. The surroundings around the car and the human body were filled with air. Furthermore, the Ella's tissues dielectric properties were chosen according to the literature [41], [42], considering the antenna working frequency of 3.5 GHz. The tissues of the human model were discretized with a maximum step of $\lambda/10$ (where $\lambda = c/f\sqrt{\varepsilon_r}$, λ is the wavelength [m], c is the speed of light [m/s], f is the wave frequency [Hz], and ε_r is the relative permittivity), depending on the tissues' dielectric properties. For this reason, the maximum mesh step was set to 1.408 mm for all body tissues apart from the eyes tissues (maximum mesh step equal to 1.043 mm). Lastly, the domain boundaries were assumed perfectly matched layer (PML) absorbing conditions. The computational simulations were conducted on a workstation with Intel®Xeon®gold 5222 CPU @3.80 GHz and with NVIDIA RTX A5000 GPU. Each deterministic simulation lasted around 7h and occupied 38,2 GB of memory.

The quantity of interest Y assessed in the computational simulations was the *SAR* for specific tissues, as indicated in the ICNIRP guidelines [33]. In particular, the *SAR* was averaged on the whole body (SAR_{wb}) and on 10g (SAR_{10g}) of tissue of the skin and the eyes (i.e., cornea, lens, sclera and humor vitreous). The values obtained through deterministic dosimetry for the SAR_{wb} and the peak of SAR_{10g} ($pSAR_{10g}$) were then used to build the surrogate models using the PC-Kriging method, as described in the next section.

C. STOCHASTIC APPROACH

As shown in Figure 2, in the Step 2 the aim was to build the surrogate model (or metamodel) for characterizing EMF exposure. A surrogate modeling technique allows to substitute the expensive computational model $M(\boldsymbol{x})$ with a metamodel for the reduction of the associated computational costs, such as:

$$\hat{Y} = \hat{M}(\boldsymbol{x}) \tag{1}$$

where $\boldsymbol{x}$ denotes the two-dimensional input vector of the two-scan angles in the H-plane and E-plane of the 5G-V2X antenna beamforming, $\hat{M}$ is the metamodel and $\hat{Y}$ represents the quantity of interest (in this case, the *SAR*) obtained with significantly lower computational cost compared to simulations with deterministic dosimetry. In this work, among the different non-intrusive approaches that can be used to obtain the metamodels, the PC-Kriging technique was selected. PC-Kriging is a novel metamodeling method formed by a universal Kriging model, whose trend is modelled by a sparse set of orthogonal polynomials. In this way, PC-Kriging allows to combine the advantages of Universal Kriging (Gaussian process modelling) with those of Polynomial Chaos Expansions (PCE), resulting in a more efficient metamodeling technique than the two methods taken separately [31], [43]. A more detailed description of the PCK technique and of PCE

and Universal Kriging methods can be found in [25], [44], and [45].

Briefly, the Universal Kriging method is a statistical interpolation method, which splits the random function into a linear combination of deterministic functions, known at any point of the domain input, and a residual random function, described by a Gaussian noise depending on the input vector. This can be represented by the following equation:

$$\hat{Y}^K = \hat{M}^K(\boldsymbol{x}) = \sum_{j=1}^{p} \beta_j f_j(\boldsymbol{x}) + Z(\boldsymbol{x}) \tag{2}$$

where $\sum_{j=1}^{p} \beta_j f_j(\boldsymbol{x})$ represents the mean value of $\hat{Y}^K$ and is a linear combination of a given functional basis f with non-zero coefficients β_j, whereas $Z(\boldsymbol{x})$ identifies the stationary Gaussian process, that captures local variations by interpolating neighboring data points of the experimental design. $Z(\boldsymbol{x})$ has zero mean and stationary autocovariance, such as:

$$E\left[Z(\boldsymbol{x}), Z\left(\boldsymbol{x}'\right)\right] = \sigma^2 R(\boldsymbol{x} - \boldsymbol{x}', \boldsymbol{\theta})\boldsymbol{x}) \tag{3}$$

where σ^2 is the constant variance of the Gaussian process, R is the stationary autocorrelation depending on the difference between the two sample points $(\boldsymbol{x} - \boldsymbol{x}')$ and the hyperparameters $\boldsymbol{\theta}$ [44].

The PCE are instead a family of powerful stochastic techniques where the computational model is functional approximated through its spectral representation based on a suitably built basis of polynomial functions. The PCE technique is described by the following equation:

$$\hat{Y}^{PCE} = \hat{M}^{PCE}(\boldsymbol{X}) = \sum_{j=1}^{p} \alpha_j \psi_j(\boldsymbol{X}) \tag{4}$$

in details, $\boldsymbol{X}$ is the probability density function associated to the input vector $\boldsymbol{x}$, p is the size of the polynomial basis $\Psi(\boldsymbol{X})$, $\psi(\boldsymbol{X})$ are the orthonormal polynomials belonging to $\Psi(\boldsymbol{X})$, and α_j are the corresponding unknown coefficients to be estimated [45].

As described before, the PC-Kriging method is a combination of the Universal Kriging with the PCE methods resulting in a more efficient technique than the two methods separately taken. The PC-Kriging can be summarized by the following equation:

$$\hat{Y}^{PCK} = \hat{M}^{PCK}(\boldsymbol{x}) = \sum_{j=1}^{p} \alpha_j \psi_j(\boldsymbol{X}) + Z(\boldsymbol{x}) \tag{5}$$

where, the first term in the equation (i.e., $\sum_{j=1}^{p} \alpha_j \psi_j(\boldsymbol{X})$) is the PCE solution and represents the trend of the model, capturing the global behavior of the model. The second term in the equation (i.e., $Z(\boldsymbol{x})$) identifies a stationary Gaussian process, that captures local variations by interpolating neighboring data points of the experimental design.

In the present work, the PC-Kriging metamodels were built using the software "UQLab: The Framework for Uncertainty Quantification" [46]. As shown in equation (5), the construction of PC-Kriging models involved then two different steps: i) the choice of the orthogonal polynomials and the estimation of unknow coefficients α_j; ii) the calibration of the Kriging model, by evaluating the variance σ^2 and the hyperparameters $\boldsymbol{\theta}$. Regarding the first step, because the values of the input vector $\boldsymbol{x}$ are uniformly distributed, we used the Legendre polynomials up to the second order as the polynomial basis and the Least Angle Regression Selection (LARS) algorithm to estimate the unknow coefficients α_j in decreasing order according to their correlations to the current residual at each LARS iteration [47].

In the second step, based on equation (3), as function R we used the Matérn correlation function and we estimated its hyperparameters σ^2 and $\boldsymbol{\theta}$ through the Cross-validation estimation and Covariance Matrix Adaptation–Evolution Strategy (CMA-ES) [31], [44]. Lastly, in the present work, we used the Optimal PC-Kriging (OPCK) metamodel that minimizes the Leave-One-Out error (LOO-Error) as the best model to jointly optimize the two parts of equation (5).

D. VALIDATION

The Step 3 is the validation of the obtained surrogate models, using the smallest number of computational simulations. In the present work, the Leave-One-Out Cross-Validation (LOO-CV) technique was applied to balance the need for minimizing the number of simulations while maintaining an acceptable error, as shown in the third step of Figure 2. This technique has previously been applied successfully to validate the metamodels describing the variability of human EMF exposure in low and high frequency scenarios [26], [28]. The LOO-CV error can be expressed by:

$$\varepsilon_{LOO-CV} = \frac{1}{N}\left[\frac{\sum_{i=1}^{N}\left(M(x_i) - \hat{M}_{(-i)}^{PCK}(x_i)\right)^2}{Var[Y]}\right] \tag{6}$$

where $M(x_i)$ represents the SAR value estimated with computational deterministic simulation in x_i, $\hat{M}_{(-i)}^{PCK}(x_i)$ denotes the same quantity but obtained with the PC-Kriging surrogate model for x_i built on all the output from the experimental design $\boldsymbol{x}$ except x_i, and $Var[Y]$ is the variance of the output results obtained from the deterministic computational simulations.

The technique is applied iteratively for the N computational deterministic simulations, to obtain the total LOO-CV error. As told before, the design set was obtained using LHS method [31]. In particular, for the present work we started from a set of N = 20 simulations and then we enrich the starting set, adding a subset of N = 10 simulations, in order to achieve an acceptable LOO-CV error. In the end, we found that N = 30 computational simulations were sufficient to guarantee a LOO-CV error below 3%.

E. EXPOSURE ASSESSMENT

In Step 4, as illustrated in Figure 2, after validating the PC-Kriging metamodels, we used them to calculate the SAR values for 1000 different combinations of the two input scan angles in the E-plane and H-plane. Indeed, as previously reported, for the 1000 beamforming patterns, we evaluated the SAR_{wb} and the peak SAR_{10g} ($pSAR_{10g}$) for the skin and

TABLE 1. LOO-CV error of the metamodels for the SAR on the whole body and for the peak SAR_{10g} on the skin and eyes tissues.

	SAR_{wb}	$pSAR_{10g}$ ON THE SKIN	$pSAR_{10g}$ ON THE EYES
LOO-CV ERROR	2.48 %	2.52 %	2.49 %

eyes tissues. The computation cost for evaluating 1000 values of *SAR* with stochastic approach were almost null and taken only few seconds. Moreover, to identify the beamforming patterns that might cause the highest exposure levels, we analyzed the percentage of *SAR* values higher than the 90% and 70% of their peak values and the corresponding H-plane and E-plane angles ranges where these latter high values occurred. Furthermore, to better characterize human exposure spatial variability we computed and analyzed the Quartile Dispersion Coefficient (QDC) for each *SAR* distribution as:

$$QDC = \frac{Q_3 - Q_1}{Q_3 + Q_1} \tag{7}$$

where Q_1 and Q_3 are respectively the first and third quartiles. Finally, in order to assess which angle, between azimuth and elevation, mostly influenced the exposure levels, a global sensitivity analysis was conducted using the Sobol variance-based method [48]. This method consists in decoupling the system output variance as the sum of the partial variances due to each input parameter. The Sobol indices of the two input scan angles in H and E planes are calculated as the ratios between the partial variances and the total variance of the system output. In this work, the software ''UQLab: The Framework for Uncertainty Quantification'' [46] was used to calculate the two first Sobol indices of the two input scan angles in H and E planes, further details about the formulas for computing Sobol indices can be found in [49]. Finally, the two calculated first Sobol indices under consideration were normalized with respect to their sum.

III. RESULTS

A. VALIDATION ERROR

Table 1 reports the LOO-CV errors for the different surrogate models of the SAR_{wb} and the $pSAR_{10g}$ in the skin and eyes as computed from the results of N = 30 computational deterministic simulations.

From Table 1, we can notice that, for all the three metamodels, the LOO-CV errors were around 2.5%, that is low enough to validate the surrogate models.

We use then the obtained surrogate models to calculate the exposure levels for 1000 different combinations of the two scan angles in the E-plane and in the H-plane of the antenna beam. The numerical results are presented in the next paragraph.

B. EMF EXPOSURE ASSESSMENT

Figures 3 - 5 show the distributions of the SAR_{wb} (Figure 3), the $pSAR_{10g}$ on the skin (Figure 4), and the $pSAR_{10g}$ on the eyes tissues (Figure 5) by varying the two scan angles of the antenna. The distributions are based on the *SAR* value calculated using the surrogate models and considering 1000 different beamforming patterns of the 5G-V2X antenna. The input power of the antenna was always set to 1 W. The right part of each figure shows the contour plot of the *SAR* distribution over the E-H plane (top panel), the contour plot of the *SAR* distribution varying the scan angle on the E-plane (middle panel) and the contour plot of the *SAR* distribution varying the scan angle on the H-plane (bottom panel).

From the three distributions illustrated in the figures 3-5 and from our analysis on the obtained *SAR* values, we observed that (i) the SAR_{wb} had a maximum value of 0.33 mW/kg, a mean value of 0.05 mW/kg and a median value of 0.02 mW/kg (ii) the highest $pSAR_{10g}$ values were found in the skin tissue, with a maximum of 9.54 mW/kg, a mean value of 2.12 mW/kg and a median value of 1.14 mW/kg, (iii) the $pSAR_{10g}$ values for the eyes tissues were slightly lower, with a maximum value of 8.69 mW/kg, a mean value of 1.21 mW/kg and a median value of 0.27 mW/kg. From these values, we can notice that the mean and median values were very similar, while the maximum values were of one order of magnitude higher than the mean and the median values, meaning that the *SAR* values are mostly concentrated in the low exposure range. Indeed, the 3D distributions and projections highlighted that the exposure levels varied greatly, depending on the beamforming pattern of the antenna. In particular, from the three projections of the right part of figure 3-5 we noticed that the highest exposure was observed when the beam of the antenna was in the range of $[-20°, +20°]$ on the azimuthal plane H and $[-20°, 0°]$ in the elevation plane E. Also, it is observed that only for a few ranges of the direction of the beam (i.e., $[-20°, +20°]$ in the H-plane and $[-20°, 0°]$ in the E-plane) the *SAR* was high, while outside these latter ranges the *SAR* was almost negligible.

Table 2 displays the percentage of values higher that the 90% and 70% of the maximum values for the three *SAR* distributions of Figures 3 to 5. It can be observed that the percentage of values higher than the 90% of the maximum *SAR* was low, ranging from 1% for the SAR_{wb} to 3.2% for the $pSAR_{10g}$ on the skin. The percentage of values greater than 70% of the maximum *SAR* increased but remained still low, reaching 4.5% for the SAR_{wb} body and 9.1% for the $pSAR_{10g}$ on the skin. This confirmed that only a small subset of the obtained values had values similar to the maximum values of the distributions. Furthermore, as previously commented for Figure 3 to Figure 5, the data in Table 2 confirm that, for all the three *SAR* distributions, the highest exposure levels were found only at very narrow scan angles of the antenna beam. In particular, for beams scanning the H-plane the highest values of the *SAR* were observed in a narrow range of scan angles symmetrically centered around 0°. The widest range was observed in the skin tissue, with almost symmetric ranges equal to $[-5°, +6°]$ for the values higher than the 90% of the maximum $pSAR_{10g}$ and $[-11°, +10°]$ for the values higher than the 70% of the maximum $pSAR_{10g}$, due to the alignment

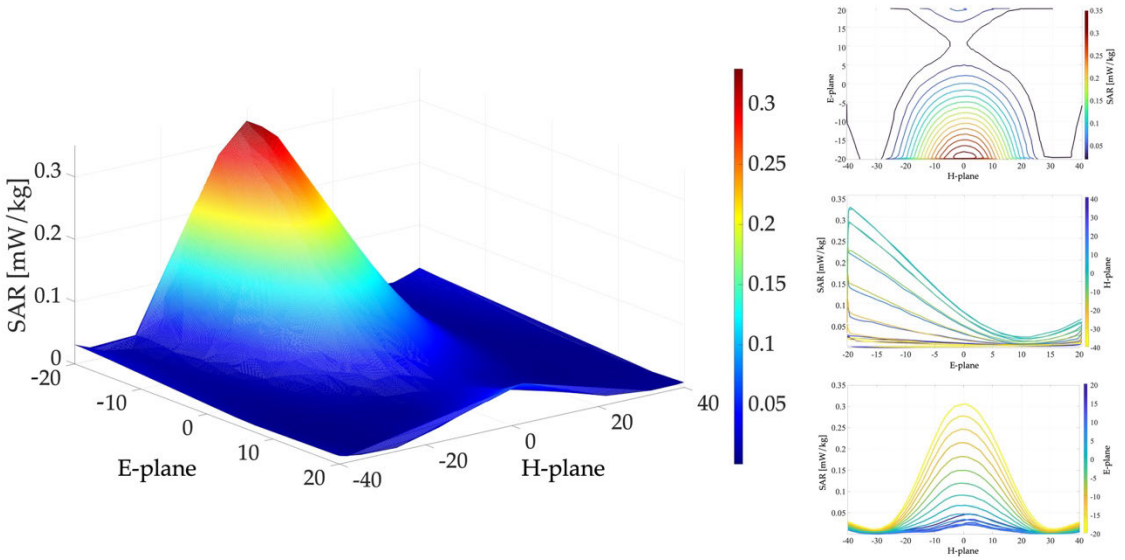

FIGURE 3. Left: SAR_{wb} levels distribution for the 1000 different combinations of the beamforming patterns of the 5G-V2X antenna. Right: in the upper part the contour map of the SAR_{wb} on the H-E plane; in the middle the contour map of the SAR_{wb} vs. the scan angle on the E-plane; in the lower part the contour map of the SAR_{wb} vs. the scan angle on the H-plane.

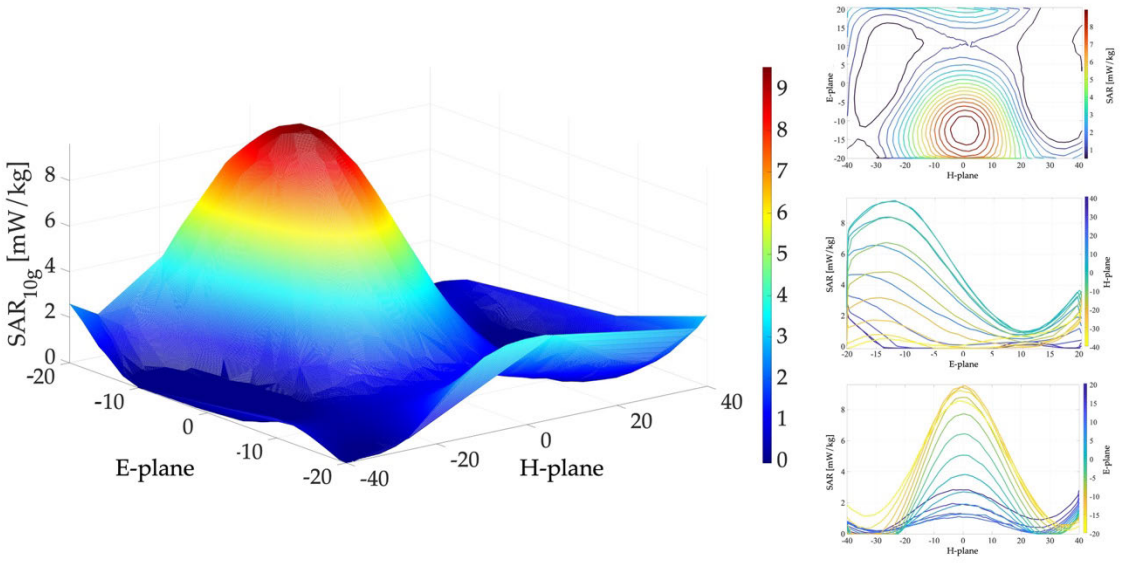

FIGURE 4. Left: $pSAR_{10g}$ levels distribution in the skin tissue for the 1000 different combinations of beamforming patterns of the 5G-V2X antenna. Right: in the upper part the contour map of the $pSAR_{10g}$ on the H-E plane; in the middle the contour map of the $pSAR_{10g}$ vs. the scan angle on the E-plane; in the lower part the contour map of the $pSAR_{10g}$ vs. the scan angle on the H-plane.

of the 5G-V2X antenna and the Ella human model, being exactly on the same line in the H-plane. On the E-plane, the highest exposure levels were obtained only for negative scanning ranges, that is when the beam was directed towards the feet of the model. Specifically, the scan range for exposures higher than 90% of the maximum *SAR* was equal to [−20°, −17°] for the whole body and the eyes tissues and to [−17°, −8°] for the skin tissue. When considering exposures higher than 70% of the maximum *SAR*, the scan range for the whole body and the eyes tissues was [−20°, −12°], while for the skin, it was equal to [−20°, −5°]. As described above, in the E-plane the highest exposures were generated when the beam was directed only towards negative scan angles. This could be explained by considering the reciprocal position between the antenna and the pedestrian. The antenna is indeed tilted at an angle of 37° on the windshield of the car; as such positive scan angles mean that the main beam of the antenna is directed upwards, beyond the head of the model, resulting in lower

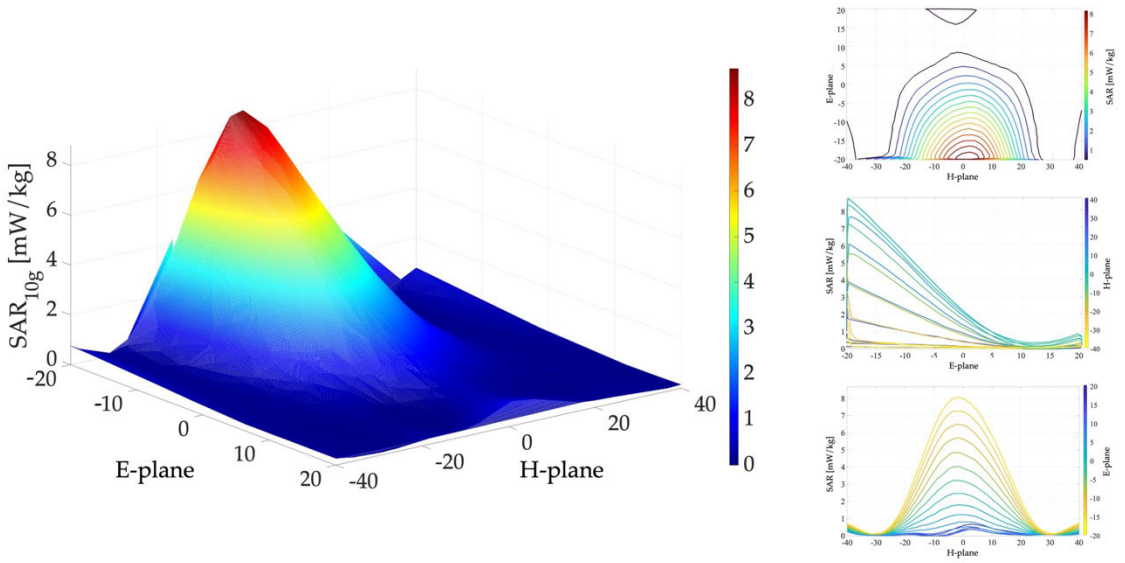

FIGURE 5. Left: $pSAR_{10g}$ levels distribution in the eyes tissue for the 1000 different combinations of beamforming patterns of the 5G-V2X antenna. Right: in the upper part the contour map of the $pSAR_{10g}$ on the H-E plane; in the middle the contour map of the SAR_{10g} vs. the scan angle on the E-plane; in the lower part the contour map of the $pSAR_{10g}$ vs. the scan angle on the H-plane.

TABLE 2. Percentage of values higher than 90% and 70% of the maximum values of the SAR for the whole body, the skin and the eyes tissues and the corresponding range of the scan angles of the antenna beam.

	SAR_{wb}	$pSAR_{10g}$ ON THE SKIN	$pSAR_{10g}$ ON THE EYES
% > 0.9 max SAR	1 %	3.2 %	1.2 %
H-plane range	[-3°, +5°]	[-5°, +6°]	[-4°, +4°]
E-plane range	[-20°, -17°]	[-17°, -8°]	[-20°, -17°]
% > 0.7 max SAR	4.5%	9.1%	4.8%
H-plane range	[-7°, +10°]	[-11°, +10°]	[-11°, 7°]
E-plane range	[-20°, -12°]	[-20°, -5°]	[-20°, -12°]

exposure levels, as the human model is only hit by the side lobes of the beam. Conversely, for negative scan angles the main beam is more directed towards the model head, causing the highest exposure levels.

The variability of the data is further supported by the QDC values we obtained, which are shown in Figure 6. As observed in Figure 6, the QDC values were high and ranged from 0.82 for the whole body to 0.88 for the eyes tissues. This means that, although low, the exposure levels change consistently as a function of the two scan angles in the H- and E-plane of the 5G-V2X antenna beamforming, introducing a high variability on the induced *SAR* levels.

In the same Figure 6, we also reported the Sobol indices from the global sensitivity analysis conducted for all the *SAR* distributions here considered. The normalized Sobol indices for the scan angle in the H-plane showed in all the three *SAR* distributions values higher than those obtained for the scan angle in the E-plane, especially for the $pSAR_{10g}$ of the skin and the eyes. For the whole body, the H- and E-plan Sobol indices were almost comparable, being 0.54 in the H-plane and 0.46 in the E-plane. For the skin and eyes tissues, the Sobol index in the H-plane was higher than that of the E-plane (0.70 vs 0.30 for the skin and 0.59 vs 0.41 for the eyes). This indicates that for the whole body, both scan angles have an almost equal impact on the exposure levels with 54% of the variance of the exposure explained by the variation of the beam direction on the H-plane and 46% of the variance explained by the variation of the beam direction on the E-plane. For the skin and the eyes tissues, the scan angle on the H-plane become more relevant than that on the E-plane, since the variation of the beam direction on the H-plane explained 70% of the variance of the exposure in the skin and 59% of the exposure in the eyes. These considerations can be explained by considering the reciprocal position between the antenna and the human model. Indeed, the wider range of variation in the H-plane could result in main beams of the 5G-V2X antenna that only partially hit the human body, causing lower exposure levels thus having a greater impact on exposure spatial variability.

IV. DISCUSSION

To the best of the authors' knowledge, this is the first study that investigated the spatial variability of human RF-EMF assessment in upcoming 5G-V2X communication scenarios. The combined use of classical computational method and the PC-Kriging stochastic approach was applied in electromagnetic dosimetry framework for C-ITS mobility scenarios, to obtain a complete description of the exposure

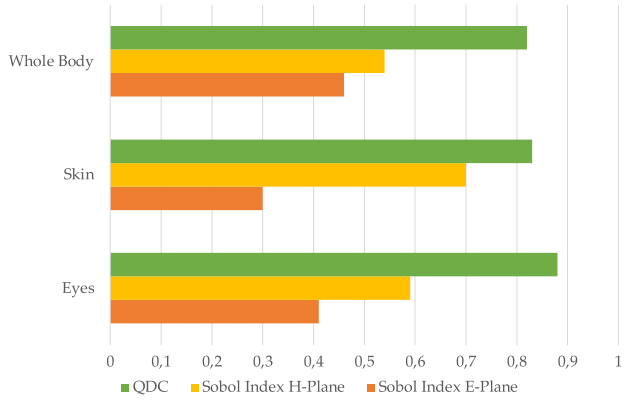

FIGURE 6. The QDC values and the normalized Sobol indices for the three SAR distributions under investigation.

heterogeneity. While the PCK (Polynomial Chaos Kriging) stochastic approach has a mono-dimensional limitation, resulting in the loss of corresponding location information about the peak exposure level on the human model, it still proves valuable in capturing EMF exposure levels' variability within next-generation 5G. Indeed, in [25], this methodology was applied for assessing different *SAR* exposure levels for a human body exposed to an indoor 5G Access Point with beamforming capability, at the working frequency of 3.7 GHz [25]. In the current study, the same method is used to assess the spatial variability of RF absorbed by a pedestrian near a car equipped with a 5G-V2X antenna at the working frequency of 3.5 GHz, in the FR1 range licensed for NR communications [24]. The 5G-V2X antenna model was based on the latest technical specifications released by 3GPP (Release 16 and 17 [7], [8]) and was mounted on the windscreen of a city car model, according to the typical antenna mounting position [36]. The spatial variability and heterogeneity of the scenario were introduced by considering a 5G-V2X antenna with beamforming capability, that was regulated by the two scan angles in the H-plane, with a variation range between $[-40°, +40°]$, and in E-plane, with a variation range between $[-20°, +20°]$. Thanks to the use of stochastic dosimetry, we were able to assess the *SAR* exposure levels of a pedestrian, for 1000 different combinations of the two scan angles, with low computational cost. The pedestrian location relative to the car was based on the position that according to the evidences we observed in our previous study [24] would cause the highest exposure levels. The human model was positioned as closest as possible to the front of the car body, since larger distances between the 5G-V2X antenna and the human body will lead to lower *SAR* levels.

Based on the 30 simulations conducted only with deterministic dosimetry, we observed that the highest *SAR* values positions were localized in the upper part of the body, particularly in the head region, with the highest exposure levels obtained in the eyes and nose area. The introduction of the PCK technique allowed us to significantly expand our analysis by considering 1000 different combinations of the two scan angles, all achieved at a low computational cost. This analysis showed that, despite the short distance between the antenna and the model, the exposure levels for the whole body, the skin, and the eyes were low and in any case below the EMF exposure limits. In fact, we found that the maximum *SAR* averaged on the whole body (SAR_{WB}) was equal to 0.33 mW/kg and the maximum peak *SAR* value averaged on 10g was 9.54 mW/kg for the skin and 8.69 mW/kg for the eyes, both well below the limits of 0.08 W/kg for the whole body *SAR* and of 2 W/kg for the local head torso *SAR*, indicated by the ICNIRP guidelines [33]. Furthermore, in realistic 5G-V2X scenarios, the antennas will be feed with value of input power around 23 dBm (i.e., 200 mW) and will work with pulsed signals and not continuous, as also indicated in the technical specification of 3GPP [7], [8]. In this way, the levels of exposure due to a V2X communication scenario will be even more significantly reduced and well below ICNIRP guidelines [33]. This result is in line with other studies, which deal with RF human exposure assessment in the context of both 5G networks and automotive field, which highlighted always values well below the EMF exposure limits [16], [17], [18], [19], [21], [22], [23], [24], [25].

Furthermore, interestingly, the obtained maximum values were slightly higher than those from our previous work [24], where we applied only the computational method and investigated the exposure only at 0° phase shift for the two scan angles. The maximum value in the worst exposure configuration of [24] was equal to 0.074 mW/kg for the whole body, 6.62 mW/kg for the $pSAR_{10g}$ on the skin, and 3.77 mW/kg for the $pSAR_{10g}$ on the eyes. The maximum of the exposure for the whole body was found at a beam angle of [0° in H-plane, −20° in E-plane], for the skin at [1° in H-plane, −13° in E-plane], and for the eyes at [0° in H-plane, −20° in E-plane]. This demonstrates that different beamforming patterns of the 5G-V2X antenna can result in higher exposure levels in different body regions, because the main beam can be more directed towards the head-eyes zone of the Ella human model, compared to the case with a 0° phase shift that we investigated in our previous work [24].

The analysis we conducted about the *SAR* values higher than the 90% and 70% of their maximum values reinforced this latter observation. Indeed, the highest values were found to concentrate in a small but symmetric scan range in the H-plane, while, in the E-plane, the highest *SAR* levels were only in the negative part of the scan range (the largest range extreme were $[-20°, -5°]$, for the whole body). This is likely due to the fact that the beamforming pattern in the positive scan range of the E-plane resulted in a main beam directed above the head of the pedestrian. Also, this result highlighted how only the beamforming patterns directed primarily towards the human model could lead to high *SAR* levels, as also underlined in our previous work that deal with exposure variability due to indoor 5G AP [25]. Moreover, the typical 5G-V2X antennas positions (i.e., on the windscreen and on the roof at the back of the car [36]), will favor beams directed upwards than the population average

height, resulting in minimal exposure for pedestrians and road users.

The QDC coefficient was always higher than 0.82. This means that, although the exposure values were low, they changed consistently, as a function of the horizontal and elevation angles of the 5G-V2X antenna beam and the exposure scenario is then characterized by a high degree of variability and heterogeneity. As previously underlined in our work [25], this was expected, since the 3D beamforming technique in 5G networks inherently focus the radiation in narrow beams to increase the gain only in the target direction and not elsewhere [11], [50]. This creates scenarios in C-ITS mobility with high variability and complexity in terms of the RF EMF exposure levels for people in close proximity.

Finally, the global sensitivity analysis based on Sobol indices showed that both the H-plane and the E-plane scan angles were relevant in affecting the induced *SAR* levels; for the skin and the eyes tissues, the scan angle in the H-plane has slightly more influence. Therefore, both azimuth and the elevation angles should be considered when developing surrogate models for accurately predicting exposure levels due to the 3D beamforming capability of a 5G-V2X antenna in a C-ITS scenario.

V. CONCLUSION

In conclusion, the PC-Kriging stochastic technique has been demonstrated to be suitable to face the spatial variability and heterogeneity of human exposure to RF EMF in the contest of smart mobility, where 5G NR communications will be soon implemented. Indeed, starting with only a few results obtained with deterministic dosimetry, in this study we could assess the exposure levels of pedestrians in close proximity to a car equipped with a 5G-V2X antenna with 3D beamforming capability. The exposure levels were evaluated in terms of the *SAR* averaged on the whole body and averaged on 10g of the skin and eyes tissues. At the end, it was shown that both the scan angles in the H-plane and E-plane had an impact on the *SAR* distributions. However, it is important to note that all the values obtained were significantly below the ICNIRP guidelines for general public exposure.

Future studies will be focused on the development of more sophisticated methods using stochastic and machine learning approaches for evaluating the exposure variables (i.e., specific absorption rate and absorbed power density) and exposure variability at RF and mm-Waves frequency ranges, considering an ever-increasing number of factors that can influence the exposure scenarios (e.g., the simultaneous presence of several sources operating at different frequencies, the morphology, the posture of the subject, etc.) [51], [52].

ACKNOWLEDGMENT

The authors would like to thank ZMT Zurich MedTech AG (www.zmt.swiss) for having provided the simulation software SIM4Life.

REFERENCES

[1] K. Sjoberg, P. Andres, T. Buburuzan, and A. Brakemeier, "Cooperative intelligent transport systems in Europe: Current deployment status and outlook," *IEEE Veh. Technol. Mag.*, vol. 12, no. 2, pp. 89–97, Jun. 2017, doi: 10.1109/MVT.2017.2670018.

[2] A. Ghosal and M. Conti, "Security issues and challenges in V2X: A survey," *Comput. Netw.*, vol. 169, Mar. 2020, Art. no. 107093, doi: 10.1016/j.comnet.2019.107093.

[3] J. Wang, Y. Shao, Y. Ge, and R. Yu, "A survey of vehicle to everything (V2X) testing," *Sensors*, vol. 19, no. 2, p. 334, Jan. 2019, doi: 10.3390/s19020334.

[4] X. Shen, R. Fantacci, and S. Chen, "Internet of Vehicles [scanning the issue]," *Proc. IEEE*, vol. 108, no. 2, pp. 242–245, Feb. 2020, doi: 10.1109/JPROC.2020.2964107.

[5] *Intelligent Transport Systems (ITS); Radiocommunications Equipment Operating in the 5 855 MHz to 5 925 MHz Frequency Band; Harmonised Standard Covering the Essential Requirements of Article 3.2 of Directive 2014/53/EU*, Standard ETSI EN 302 571, Version 2.1.1, 2017.

[6] A. Bazzi, G. Cecchini, M. Menarini, B. M. Masini, and A. Zanella, "Survey and perspectives of vehicular Wi-Fi versus sidelink cellular-V2X in the 5G era," *Future Internet*, vol. 11, no. 6, p. 122, 2019, doi: 10.3390/fi11060122.

[7] *Technical Specification Group Radio Access Network; NR Sidelink Enhancement; User Equipment (UE) Radio Transmission and Reception; (Release 17)*, document 3GPP TR 38.785, Version 0.3.0, 2021.

[8] *Technical Specification Group Radio Access Network; V2X Services based on NR; User Equipment (UE) Radio Transmission and Reception; (Release 16)*, document 3GPP TR 38.886, Version 16.3.0, 2021.

[9] *5GCAR Deliverable D2.1: 5GCAR Scenarios, Use Cases, Requirements and KPIs*, Version 2.0, Feb. 2019.

[10] W. H. Chin, Z. Fan, and R. Haines, "Emerging technologies and research challenges for 5G wireless networks," *IEEE Wireless Commun.*, vol. 21, no. 2, pp. 106–112, Apr. 2014, doi: 10.1109/MWC.2014.6812298.

[11] S. M. Razavizadeh, M. Ahn, and I. Lee, "Three-dimensional beamforming: A new enabling technology for 5G wireless networks," *IEEE Signal Process. Mag.*, vol. 31, no. 6, pp. 94–101, Nov. 2014, doi: 10.1109/MSP.2014.2335236.

[12] J. T. Bushberg, C. K. Chou, K. R. Foster, R. Kavet, D. P. Maxson, R. A. Tell, and M. C. Ziskin, "IEEE committee on man and radiation—COMAR technical information statement: Health and safety issues concerning exposure of the general public to electromagnetic energy from 5G wireless communications networks," *Health Phys.*, vol. 119, no. 2, pp. 236–246, Aug. 2020, doi: 10.1097/HP.0000000000001301.

[13] C. L. Bamy, F. M. Mbango, D. B. O. Konditi, and P. M. Mpele, "A compact dual-band dolly-shaped antenna with parasitic elements for automotive radar and 5G applications," *Heliyon*, vol. 7, no. 4, Apr. 2021, Art. no. e06793, doi: 10.1016/j.heliyon.2021.e06793.

[14] A. Pfadler, C. Ballesteros, J. Romeu, and L. Jofre, "Hybrid massive MIMO for urban V2I: Sub-6 GHz vs mmWave performance assessment," *IEEE Trans. Veh. Technol.*, vol. 69, no. 5, pp. 4652–4662, May 2020, doi: 10.1109/TVT.2020.2982743.

[15] S. Hasturkoglu and S. Lindenmeier, "Antenna module with new wideband 5G-antenna array at 28 GHz in combination with GNSS- and 4G/WLAN/DSRC in automotive environment," in *Proc. 48th Eur. Microw. Conf. (EuMC)*, Madrid, Spain, Sep. 2018, pp. 1073–1076, doi: 10.23919/EuMC.2018.8541591.

[16] M. S. Morelli, S. Gallucci, B. Siervo, and V. Hartwig, "Numerical analysis of electromagnetic field exposure from 5G mobile communications at 28 GHZ in adults and children users for real-world exposure scenarios," *Int. J. Environ. Res. Public Health*, vol. 18, no. 3, p. 1073, Jan. 2021, doi: 10.3390/ijerph18031073.

[17] R. Morimoto, A. Hirata, I. Laakso, M. C. Ziskin, and K. R. Foster, "Time constants for temperature elevation in human models exposed to dipole antennas and beams in the frequency range from 1 to 30 GHz," *Phys. Med. Biol.*, vol. 62, no. 5, pp. 1676–1699, Mar. 2017, doi: 10.1088/1361-6560/aa5251.

[18] I. Laakso, R. Morimoto, J. Heinonen, K. Jokela, and A. Hirata, "Human exposure to pulsed fields in the frequency range from 6 to 100 GHz," *Phys. Med. Biol.*, vol. 62, no. 17, p. 6980, Aug. 2017.

[19] B. Thors, D. Colombi, Z. Ying, T. Bolin, and C. Törnevik, "Exposure to RF EMF from array antennas in 5G mobile communication equipment," *IEEE Access*, vol. 4, pp. 7469–7478, 2016, doi: 10.1109/ACCESS.2016.2601145.

[20] E. Baramili, R. Sarkis, and M. B. Saleh, "Investigation of driver EMF exposure from 4G/5G automotive glass mounted antennas," in *Proc. IEEE Int. Symp. Antennas Propag. North Amer. Radio Sci. Meeting*, Montreal, QC, Canada, Jul. 2020, pp. 1451–1452, doi: 10.1109/IEEECONF35879.2020.9329845.
[21] G. Tognola, M. Bonato, M. Benini, S. Aerts, S. Gallucci, E. Chiaramello, S. Fiocchi, M. Parazzini, B. M. Masini, W. Joseph, J. Wiart, and P. Ravazzani, "Survey of exposure to RF electromagnetic fields in the connected car," *IEEE Access*, vol. 10, pp. 47764–47781, 2022.
[22] G. Tognola, B. Masini, S. Gallucci, M. Bonato, S. Fiocchi, E. Chiaramello, M. Parazzini, and P. Ravazzani, "Numerical assessment of RF human exposure in smart mobility communications," *IEEE J. Electromagn., RF Microw. Med. Biol.*, vol. 5, no. 2, pp. 100–107, Jun. 2021, doi: 10.1109/JERM.2020.3009856.
[23] M. Benini, M. Parazzini, M. Bonato, S. Gallucci, E. Chiaramello, S. Fiocchi, and G. Tognola, "Road user exposure from ITS-5.9 GHz vehicular connectivity," *Sensors*, vol. 22, no. 18, p. 6986, Sep. 2022, doi: 10.3390/s22186986.
[24] M. Bonato, G. Tognola, M. Benini, S. Gallucci, E. Chiaramello, S. Fiocchi, and M. Parazzini, "Assessment of SAR in road-users from 5G-V2X vehicular connectivity based on computational simulations," *Sensors*, vol. 22, no. 17, p. 6564, Aug. 2022, doi: 10.3390/s22176564.
[25] M. Bonato, L. Dossi, E. Chiaramello, S. Fiocchi, G. Tognola, and M. Parazzini, "Stochastic dosimetry assessment of the human RF-EMF exposure to 3D beamforming antennas in indoor 5G networks," *Appl. Sci.*, vol. 11, no. 4, p. 1751, Feb. 2021.
[26] M. Bonato, E. Chiaramello, S. Fiocchi, G. Tognola, P. Ravazzani, and M. Parazzini, "Influence of low frequency near-field sources position on the assessment of children exposure variability using stochastic dosimetry," *IEEE J. Electromagn., RF Microw. Med. Biol.*, vol. 4, no. 3, pp. 179–186, Sep. 2020, doi: 10.1109/JERM.2019.2958549.
[27] E. Chiaramello, S. Fiocchi, P. Ravazzani, and M. Parazzini, "Stochastic dosimetry for the assessment of children exposure to uniform 50 Hz magnetic field with uncertain orientation," *BioMed Res. Int.*, vol. 2017, pp. 1–14, Oct. 2017, doi: 10.1155/2017/4672124.
[28] E. Chiaramello, S. Fiocchi, M. Parazzini, P. Ravazzani, and J. Wiart, "Stochastic dosimetry for radio-frequency exposure assessment in realistic scenarios," in *Uncertainty Modeling for Engineering Applications* (PoliTO Springer Series), F. Canavero, Eds. Cham, Switzerland: Springer, 2019, pp. 89–102, doi: 10.1007/978-3-030-04870-9_6.
[29] J. Silly-Carette, D. Lautru, M.-F. Wong, A. Gati, J. Wiart, and V. F. Hanna, "Variability on the propagation of a plane wave using stochastic collocation methods in a bio electromagnetic application," *IEEE Microw. Wireless Compon. Lett.*, vol. 19, no. 4, pp. 185–187, Apr. 2009.
[30] O. Jawad, D. Lautru, A. Benlarbi-Delai, J. M. Dricot, F. Horlin, and P. De Doncker, "A human body model exposed to a cluster of waves: A statistical study of SAR," *Prog. Electromagn. Res. C*, vol. 30, pp. 1–13, 2012, doi: 10.2528/PIERC12030804.
[31] P. Kersaudy, B. Sudret, N. Varsier, O. Picon, and J. Wiart, "A new surrogate modeling technique combining Kriging and polynomial chaos expansions—Application to uncertainty analysis in computational dosimetry," *J. Comput. Phys.*, vol. 286, pp. 103–117, Apr. 2015, doi: 10.1016/j.jcp.2015.01.034.
[32] M. A. Hajj, S. Wang, P. D. Doncker, C. Oestges, and J. Wiart, "A statistical estimation of 5G massive MIMO's exposure using stochastic geometry," in *Proc. XXXIII Gen. Assem. Sci. Symp. Int. Union Radio Sci.*, Aug. 2020, pp. 1–3.
[33] International Commission on Non-Ionizing Radiation Protection, "Guidelines for limiting exposure to electromagnetic fields (100 kHz to 300 GHz)," *Health Physics*, vol. 118, no. 5, pp. 483–524, May 2020, doi: 10.1097/HP.0000000000001210.
[34] *H2020 5G PPP 5GCar Project*. Accessed: Jun. 8, 2023. [Online]. Available: https://5gcar.eu
[35] G. Artner, W. Kotterman, G. D. Galdo, and M. A. Hein, "Automotive antenna roof for cooperative connected driving," *IEEE Access*, vol. 7, pp. 20083–20090, 2019.
[36] T. Adam, S. Kopp, S. Lang, and A. Winkelmann, "V2X—An important building block in cooperative intelligent transport systems (C-ITS)," TE Commun. V2X, Tech. Rep., 2019. [Online]. Available: https://www.te.com/content/dam/te-com/documents/automotive/global/automotive-next-gen-mobility-v2x-62309-2019-en.pdf
[37] *Technical Specification Group Radio Access Network; Study on New Radio Access Technology Physical Layer Aspects (Release 14)*, document 3GPP TR 38.802, Version 14.2.0, Sep. 2017. [Online]. Available: http://www.3gorg
[38] M.-C. Gosselin, E. Neufeld, H. Moser, E. Huber, S. Farcito, L. Gerber, M. Jedensjö, I. Hilber, F. D. Gennaro, B. Lloyd, E. Cherubini, D. Szczerba, W. Kainz, and N. Kuster, "Development of a new generation of high-resolution anatomical models for medical device evaluation: The virtual population 3.0," *Phys. Med. Biol.*, vol. 59, no. 18, pp. 5287–5303, Sep. 2014, doi: 10.1088/0031-9155/59/18/5287.
[39] G. Blatman, "Adaptive sparse polynomial chaos expansions for uncertainty propagation and sensitivity analysis," Doctoral dissertation, Université Blaise Pascal, Clermont-Ferrand, France, 2009.
[40] A. Taflove, S. C. Hagness, and M. Piket-May, "Computational electromagnetics: The finite-difference time-domain method," in *The Electrical Engineering Handbook*. Amsterdam, The Netherlands: Elsevier, 2004, p. 3.
[41] C. Gabriel, S. Gabriel, and E. Corthout, "The dielectric properties of biological tissues: I. Literature survey," *Phys. Med. Biol.*, vol. 41, no. 11, pp. 2231–2249, Nov. 1996, doi: 10.1088/0031-9155/41/11/001.
[42] S. Gabriel, R. W. Lau, and C. Gabriel, "The dielectric properties of biological tissues: II. Measurements in the frequency range 10 Hz to 20 GHz," *Phys. Med. Biol.*, vol. 41, no. 11, pp. 2251–2269, Nov. 1996, doi: 10.1088/0031-9155/41/11/002.
[43] R. Schobi, B. Sudret, and J. Wiart, "Polynomial-chaos-based Kriging," *Int. J. Uncertainty Quantification*, vol. 5, no. 2, pp. 171–193, 2015.
[44] C. Lataniotis, D. Wicaksono, S. Marelli, and B. Sudret, "UQLab user manual—Kriging (Gaussian process modeling)," Chair Risk, Saf. Uncertainty Quantification, ETH, Zurich, Switzerland, Tech. Rep. UQLab-V1.3-105, 2019.
[45] B. Sudret, "Uncertainty propagation and sensitivity analysis in mechanical models—Contributions to structural reliability and stochastic spectral methods," Habilitationa Diriger des Recherches, Université Blaise Pascal, Clermont-Ferrand, France, Tech. Rep., 2007, p. 147.
[46] S. Marelli and B. Sudret, "UQLab: A framework for uncertainty quantification in MATLAB," in *Proc. 2nd Int. Conf. Vulnerability Risk Anal. Manag. (ICVRAM), 6th Int. Symp. Uncertainty Modeling Anal.*, 2015, pp. 2554–2563.
[47] B. Efron, T. Hastie, I. Johnstone, and R. Tibshirani, "Least angle regression," *Ann. Stat.*, vol. 32, no. 2, pp. 407–499, 2004.
[48] I. M. Sobol, "Global sensitivity indices for nonlinear mathematical models and their Monte Carlo estimates," *Math. Comput. Simul.*, vol. 55, nos. 1–3, pp. 271–280, Feb. 2001.
[49] S. Marelli, C. Lamas, K. Konakli, C. Mylonas, P. Wiederkehr, and B. Sudret, "UQLab user manual—Sensitivity analysis," Tech. Rep. UQLab-V1, 2019, pp. 2–106.
[50] J. Jang, M. Chung, S. C. Hwang, Y.-G. Lim, H.-J. Yoon, T. Oh, B.-W. Min, Y. Lee, K. S. Kim, C.-B. Chae, and D. K. Kim, "Smart small cell with hybrid beamforming for 5G: Theoretical feasibility and prototype results," *IEEE Wireless Commun.*, vol. 23, no. 6, pp. 124–131, Dec. 2016, doi: 10.1109/MWC.2016.1500387WC.
[51] T. Mazloum, S. Wang, M. Hamdi, B. A. Mulugeta, and J. Wiart, "Artificial neural network-based uplink power prediction from multi-floor indoor measurement campaigns in 4G networks," *Frontiers Public Health*, vol. 9, Nov. 2021, Art. no. 777798.
[52] Y. Jiang, H. Wang, X. Sun, C. Li, and T. Wu, "Evaluation of Chinese populational exposure to environmental electromagnetic field based on stochastic dosimetry and parametric human modelling," *Environ. Sci. Pollut. Res.*, vol. 30, no. 14, pp. 40445–40460, Jan. 2023.

MARTA BONATO received the master's degree in biomedical engineering from the Polytechnic of Milano, Milan, Italy, in July 2017, where she is currently pursuing the Ph.D. degree in bioengineering. From September 2017 to April 2018, she was with the Institute of Electronics, Computer and Telecommunication Engineering, Consiglio Nazionale delle Ricerche, as a Research Fellow. Her current research interests include the study of the interaction of electromagnetic fields (EMF) with biological systems and the study of possible effects of EMF on health with both deterministic and stochastic dosimetry, particularly from 5G mobile communications.

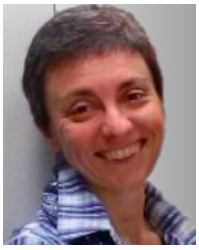

GABRIELLA TOGNOLA received the master's degree in electronic engineering and the Ph.D. degree in bioengineering from Politecnico di Milano, Milan, Italy. She is currently a Senior Research Scientist with the Institute of Electronics, Computer and Telecommunication Engineering, Consiglio Nazionale delle Ricerche. Her current research interests include exposure assessment of electromagnetic fields with numerical dosimetry and with machine learning methods and the modeling of electromagnetic fields for biomedical applications.

MARTINA BENINI (Graduate Student Member, IEEE) received the B.S. degree in biomedical engineering from Alma Mater Studiorum—Universitàì di Bologna, Italy, in 2017, and the M.S. degree in biomedical engineering from Politecnico di Milano, Italy, in 2020, where she is currently pursuing the Ph.D. degree in bioengineering. From October 2020 to April 2021, she was a Research Fellow with the Institute of Electronics, Information Engineering and Telecommunications (IEIIT), Consiglio Nazionale delle Ricerce (CNR). Her current research interests include the study of the interaction between the electromagnetic fields (EMFs) and the human body with both deterministic and stochastic dosimetry, with a focus on the antennas used in the automotive field for vehicular connectivity.

SILVIA GALLUCCI received the master's degree in biomedical engineering from the University of Pisa, Italy, in 2019, and the Ph.D. degree in bioengineering from Politecnico di Milano, with a focus on the EMF-human interactions. From December 2019 to April 2020, she was a Research Fellow with the Institute of Electronics, Computer and Telecommunication Engineering, Consiglio Nazionale delle Ricerche. Her current research interest includes the exposure assessment of electromagnetic fields with numerical dosimetry, particularly from 5G mobile communications.

EMMA CHIARAMELLO received the master's and Ph.D. degrees in biomedical engineering from Politecnico di Torino, Torino, Italy, in 2009 and 2013, respectively. She is currently a Research Scientist with the Institute of Electronics, Computer, and Telecommunication Engineering, National Research Council of Italy, Rome, Italy. Her current research interests include the study of the interactions between EMF and biological systems, with both deterministic dosimetry based on computational electromagnetism methods and stochastic dosimetry based on surrogate modeling.

SERENA FIOCCHI received the master's degree in biomedical engineering and the Ph.D. degree in bioengineering from the Polytechnic University of Milan, Milan, Italy, in 2009 and 2014, respectively. She is currently a Research Scientist with the Institute of Electronics, Computer, and Telecommunication Engineering, National Research Council of Italy, Rome, Italy. Her current research interests include the study of the computational modeling of non- invasive brain and spinal stimulation techniques, the design and the optimization of biomedical technologies based on electromagnetic fields (EMF) for diagnostic and therapeutic applications, and the computational modeling of the interactions between EMF and biological systems.

MARTA PARAZZINI (Member, IEEE) is currently a Research Scientist with the Institute of Electronics, Computer, and Telecommunication Engineering, Italian National Research Council, Rome, Italy. Her current research interests include the study of the interactions of EMF with biological systems, deterministic and stochastic computational dosimetry, and the medical applications of EMF, in particular the techniques for noninvasive brain stimulation.

Open Access funding provided by 'Consiglio Nazionale delle Ricerche-CARI-CARE-ITALY' within the CRUI CARE Agreement